CARBON MULTI-NANOTUBES FIBER FOR RTM-PROCESSED COMPOSITES

V. Lutz[1*], N. Godin[2], F. Lortie[1], J. Duchet-Rumeau[1], J. F. Gerard[1]

[1]*Université de Lyon, F-69003 Lyon, INSA Lyon, Ingénierie des Matériaux Polymères, UMR CNRS 5223, 17 Avenue Jean Capelle, F-69621 Villeurbanne, France*
[2] *Université de Lyon, F-69003 Lyon, INSA Lyon, MATEIS, 7 Avenue Jean Capelle, F-69621 Villeurbanne, France*
**vincent.lutz@insa-lyon.fr*

Keywords: polymer-matrix composite, CNT fiber, fragmentation, acoustic emission

Abstract
A commercial T700S carbon fiber and a CNT fiber obtained by direct spinning are compared for their ability to form a strong carbon/epoxy interface, through use of single-fiber-fragmentation testing, acoustic emission, transmission optical and electron microscopy. Typical microfailure modes including fiber break, matrix crack and debonds have been observed for T700S specimen. On the contrary, CNT fiber specimen seemed to stay unaffected under tensile test prior to matrix failure. However, acoustic emission results show significant differences between the 2 types of fibers and could be a useful tool for evaluating the quality of CNT fiber-epoxy interface.

1 Introduction

Nowadays, polymer-matrix composites reinforced with carbon fibers are increasingly used in the whole transport sector (aerospace, automotive and railway industries). However, the obtained parts still suffer from low impact resistance and low damage tolerance. To improve these properties, the matrix precursors have to be combined with organic or inorganic compounds to lead to multi-phased matrices. Among them, CNT are especially promising for targeting multi-scale reinforcement [1,2].
Since high quality of the parts are required, continuous-fibers-reinforced composites can be produced by resin transfer molding (RTM) which also offers a reduced cost if compared with high temperature and high pressure processes. However, RTM requires a very low viscosity of the polymer precursors and CNT-filled precursors (even at low CNTs contents) are far too viscous to be injected on dry performs. In addition, this strategy does not allow for a control of the CNTs dispersion, location and orientation in the final part. In recent years, innovative ways were studied to insert CNTs in the mold with local positioning and defined orientation. Sun et al. showed that partially cured epoxy/SWCNT thin film can be used to place CNTs at location of interest to reinforce resin-transfer-molded composites [3]. Cheng et al. investigated CNT/epoxy composites made with CNT sheets drawn from super-aligned CNT arrays. These composites with homogenous dispersion, high loading, and controllable orientation were successfully manufactured by a RTM process. Mechanical and electrical properties of these composites were significantly improved, compared to other literature references [4].

An alternative route towards CNT-based composites with superior properties consists in using pure CNT fibers or yarns, as well as carbon fibers. Chou et al. and Park et al. reviewed recently the three different production methods of CNT fibers: forest spinning, direct spinning and solution spinning [5,6]. The high mechanical properties along the CNT axis make them ideal candidates for achieving multiscale reinforcement in polymer matrices [7-12]. Pure CNT fibers can also lead to lightweight multifunctional composites [13,14].
The mechanical behavior of composites doesn't depend only on the properties of the constituent materials. In particular, the nature of the interfacial adhesion and the load transfer from the matrix to the fiber through shear play an important role. Interfacial shear strength (IFSS) is generally one of the main factors to determine mechanical performance of continuous fiber reinforced composites, however only a few studies have been focused on the CNT fiber/matrix interface. The measurement of single fiber interfacial properties requires special micro-mechanical techniques as follows: the micro-indentation, the single fiber fragmentation test and the single fiber microdroplet test (which is also called the single fiber pull-out test) [15]. The interfacial shear strength of a CNT fiber in an epoxy matrix has been recently characterized by a single fiber fragmentation test [16] and then by a microdroplet test [17]. The CNT fibers investigated in these studies were dry spun by drawing and twisting the CNT strip out of the array (forest spinning). Differences of CNT fiber diameter, microstructure and spinning methods may affect the inter CNT, inter-CNT bundle load transfer and the fiber/matrix interface. To our knowledge, CNT fibers which are obtained by direct spinning and under investigation in this study have never been characterized by such techniques so far.

2 Experimental

2.1 Materials

The fibers used in this study are T700S carbon fibers from Toray and CNT fiber from University of Cambridge. T700S fibers with "5" surface sizing (1% sizing content) is designed by the manufacturer to be compatible with epoxy precursors. CNT fibers were produced by direct spinning of a CNT aerogel directly from the gas-phase during CNT growth by chemical vapor deposition, using thiophene, ferrocene and methane as precursors and hydrogen as a carrier gas [18]. The fibers are collected at rates of 30m/min and then condensed by spraying with acetone [7]. The fibers are then combined with RTM6-2, an epoxy thermoset system, supplied by Hexcel Composites. RTM6-2 is a commercially bi-component epoxy-amine system, specially developed to fulfill the requirements of the aerospace composites industry.

2.2 Specimen preparation

Dog-bone shape specimens for fragmentation test were obtained by casting the liquid thermoset precursors into rubber molds with a single carbon fiber or single CNT fiber mounted along the center line of the cavity as shown in Figure 1. The mold itself was used to clamp the single fiber at both ends. The liquid thermoset precursors into the mold were then degassed at 100 °C during 30 min in a vacuum chamber. The test specimens were pre-cured for 90 min at 140 °C and then post-cured at 180 °C for 2 h. Three types of specimens were produced: pure RTM6-2 matrix, single carbon fiber T700SC in RTM6-2 and single CNT fiber in RTM6-2. Each kind of specimens was tested several times, and representative's results are described in this paper.

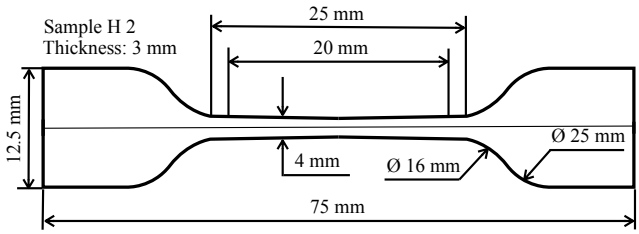

Figure 1. Dimensions of a dog-bone-shaped single fiber fragmentation specimen

2.3 Mechanical testing

Testing machine (L/M MTS) with a load cell of 10 kN was used to perform the single fiber fragmentation tests at a cross-head speed of 0.5 mm/min and at room temperature. The post-cure observation of the matrix/CNT fiber specimen was performed by transmission electron microscopy with a PHILIPS CM 120 device, at an acceleration voltage of 80 kV. Ultramicrotomy has been used to prepare TEM samples with a thickness of 70nm. Optical microscopy (ZEISS Axiophot) was used to count fiber fragmentations and analyze the morphologies after tensile tests.

2.4 Acoustic emission

Acoustic emission (AE) was continuously monitored during the tensile tests by using a Mistras 2001 data acquisition system of Physical Acoustics Corporation (PAC), with a sampling rate of 8 MHz and a 40 dB pre-amplification. Ambient noise was filtered by applying a threshold of 32 dB. AE measurements were achieved by using two resonant nano-30 PAC sensors, which have a large range of resonance (100-800 kHz), coupled on the sample surface with silicon grease. Figure 2 shows the surface localization of the sensors during tensile tests. After the installation of the transducers, a pencil lead break procedure [19] was used to simulate AE signals in the calibration of each test. In this test, a repeatable acoustic wave can be generated. When the lead breaks, there is a sudden release of stress on the surface of the sample causing an acoustic wave. Preliminary measurements allowed us to set up the acquisition parameters for our materials (peak definition time = 40 μs; hit definition time = 80 μs; hit lock time = 1000 μs) and to measure the mean wave speed for each sample to achieve the linear localization of AE sources. The difference in arrival times between the two sensors was deduced from the first peaks detected. This velocity determination procedure was repeated several times and at different positions between the sensors to ensure the accuracy of the measure wave speed. The velocity was found to be equal to 1850 m/s for the pure matrix, 2050 m/s for the carbon fiber and 1700 m/s for the CNT fiber.

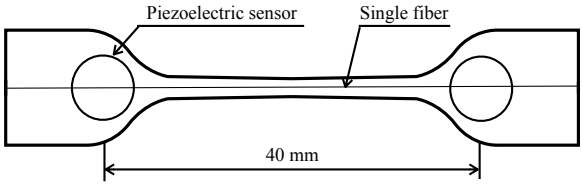

Figure 2. Sensors localization on the specimen during tensile test

3 Results and discussion

3.1 Transmission optical microscopy and transmission electron microscopy investigations

The modes of failure at fiber breaks are affected by interfacial adhesion. Figure 3 shows micrographs of two fiber breaks sites for T700S carbon fiber in the RTM6-2 matrix using

transmitted unpolarized and polarized light. Matrix cracks were induced at the fiber break sites as it was expected for treated and sized T700/epoxy system [20]. Figure 4 shows two different kind of fiber breaks, always coupled with matrix cracks. The magnified failure modes and stress whitening distribution called birefringence around a fiber break are also observed. The photoelastic birefringence patterns of shear stress are indicative of fiber matrix interface quality [21]. In our case, the kind of birefringence pattern proves that the T700 fiber strongly interacts with the matrix, although the T700S/RTM6-2 composite specimen failed before reaching saturation due to the brittle nature of RTM6-2 matrix. In fact, the energy, which is released upon fiber breaks, tends to affect the matrix region instead of altering the fiber/matrix interface. Only a short debonding zone (20 µm) was noticed around the fiber break.

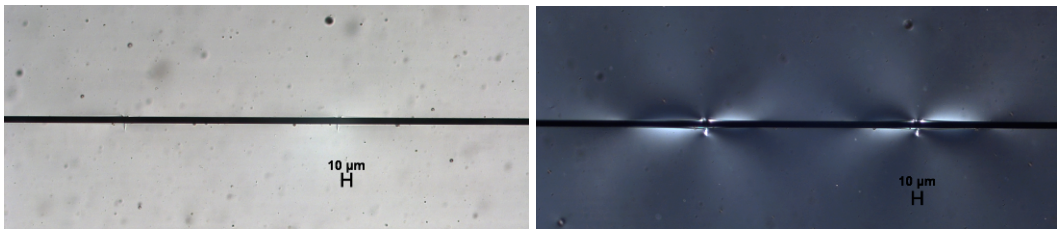

Unpolarized **Polarized**

Figure 3. Transmission optical micrograph (20x) of two T700S carbon fiber/RTM6-2 composites

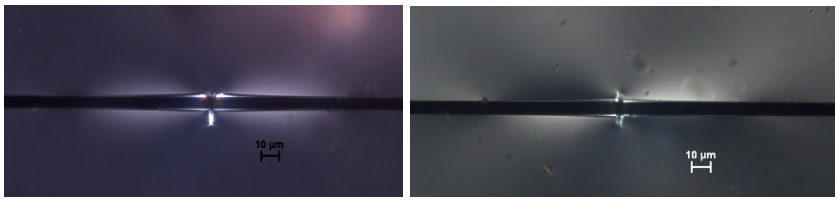

Figure 4. Transmission optical micrograph (40x) of T700S carbon fiber in RTM6-2 matrix

The pure CNT fiber (≈10 µm diameter) observed after tensile test is shown in Figure 5. No fiber break and no debonding region were observed after composite failure. This result is not surprising since, as reported in the literature, the elongation at break of a CNT fiber is more than twice the value for carbon fiber [7,22]. It seems that a strong interface between the CNT fiber and RTM6-2 was generated during specimen fabrication. As reported by Vilatela et al. and Mora et al., the high internal area of CNT fibers is accessible to polymer molecules, polymer diffusion occurs driven by capillary forces thanks to its yarn-like structure [23,24]. As shown on Figure 6, the voids, which previously existed between CNT bundles, in the internal structure of CNT fiber appear to be completely filled by RTM6-2 thermoset. Some impurities (amorphous carbon) and residual iron can also be observed on the CNT fiber cross section.

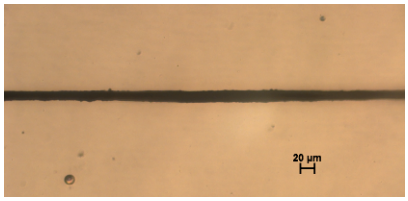

Figure 5. Transmission optical micrograph (20x) of pure and unsized CNT fiber in RTM6-2 matrix

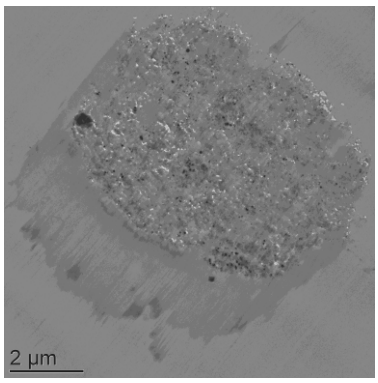

Figure 6. Transmission electron micrograph of CNT fiber, showing its cross section after RTM6-2 infiltration and polymerization

3.2 Acoustic emission analyses

In addition to direct observation of fragmentation by means of an optical microscope, acoustic emission analyses for the three kinds of specimens were monitored. Godin et al. associated acoustic events with fiber breaks collected during tensile tests on single-glass-fiber/polyester composite [25]. AE events are localized signals occurring in the gage length while AE hits refer to all detected signals (localized and unlocalized). The location of AE events, taking the middle position of the gage length as reference point, is plotted versus the strain in Figure 7. AE events were distributed over the entire gage length. Table 1 shows the correspondence between the number of acoustic events and the number of fiber breaks determined by post-test optical microscopy, for two different T700S single fiber specimen in RTM6-2 matrix. A one-to-one correlation between the number of acoustic events and the number of fiber breaks detected with a polarizing microscope has been established. It confirms that the AE events can be attributed to fiber breaks. Tests were deliberately run at a moderately slow speed to avoid the problem of multiple fiber breaks per acoustic event, which would lower the acoustically amount of detected fiber fractures.

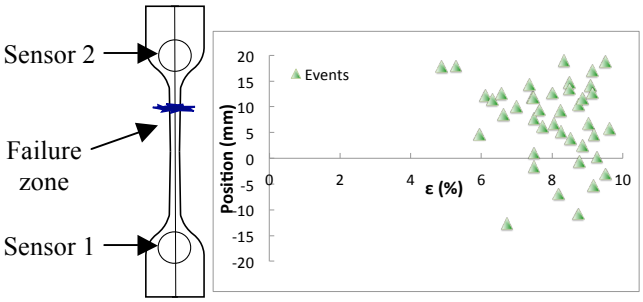

Figure 7. Location of the AE events occurring in the gage length for a T700S single fiber/RTM6-2 composite

	Specimen n°1	Specimen n°2
Number of fiber breaks observed by microscopy	38	11
Number of AE events detected by acoustic emission	41	12

Table 1. Fiber breaks correspondence for two T700S single fiber/RTM6-2 composites

Stress/strain curves and AE activities are represented on Figure 8 for three representative specimens for each kind of composites. Important AE activity of neat RTM6-2 specimen is recorded, due to the highly cross-linked polymer network, which breaks during tensile test. Initiation period starts in the elastic domain for neat RTM6-2 and T700S carbon fiber

composite, indicating the early state of damage, whereas the CNT fiber composite initiation period occurs at the beginning of the plastic domain, up to 2% of strain. A noticeable increase in AE activity is detected at around 6% of strain for the three different types of specimen. Then the emission increases significantly until the final composite failure. The T700S carbon fiber composite activity is significantly higher than that of the CNT fiber composite. In fact, besides the single matrix activity, this result can be explained by the presence of the three different failure modes during the tensile test, which are all signatures of the fiber/matrix interface behavior. Fiber breaks which can be followed by matrix cracks and debonding regions, occurring at different time, are all potential sources of AE signals. Furthermore, independent matrix cracks and debonds without preexisting fiber break may also happen in the T700S carbon fiber composite.

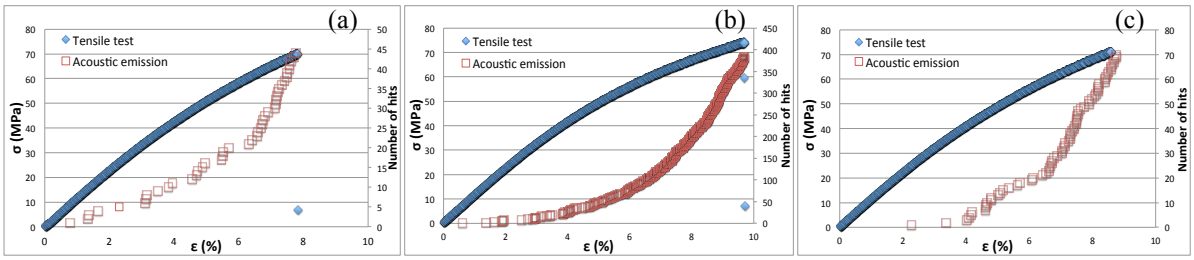

Figure 8. Stress/strain curve with acoustic emission activity for neat RTM6-2 sample (a), T700S single fiber/RTM6-2 composites (b) and CNT single fiber/RTM6-2 composites (c)

The amplitudes distributions of the collected hits are quite identical between neat epoxy and CNT fiber composite, as observed in Figure 9 (a) and (c). However, accumulated hits between 35 and 60 dB are mainly detected at 6% of strain for the CNT fiber composite. Moreover, as we can see on Figure 8 (a) and (c), the CNT fiber activity is 30 % higher than that of neat epoxy matrix. These facts could be explained by a possible alignment of CNT bundles in the CNT fiber, a possible interface effect between CNT bundles and infiltrated epoxy matrix, and inter double-walled CNT load transfer. Figure 9 (b) shows the amplitude of the localized T700S carbon fiber breaks events and hits referring to all the other signals. It has to be mentioned that fiber breaks events were still detected when the composite failed, so it means that the saturation of T700S carbon fiber breaks was not reached at the end of the test. No quantitative values of interfacial shear strength can be deduced from these experiments.

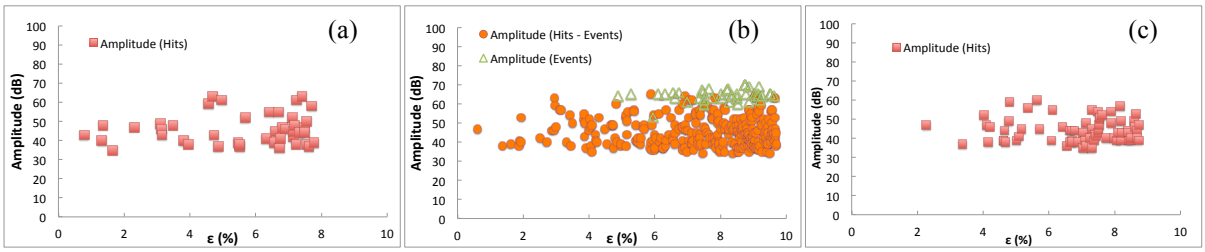

Figure 9. Acoustic emission activity curve with amplitude distribution as a function of strain for neat RTM6-2 sample (a), T700S single fiber/RTM6-2 composites (b) and CNT single fiber/RTM6-2 composites (c)

The amplitudes of the collected T700S carbon fiber signals are mainly distributed in two zones exhibiting a bimodal behavior, as represented in Figure 10 (b). About 80% of them have amplitudes in the range of 30-60 dB, same range as for the RTM6-2 matrix in Figure 10 (a). The 20% left signals have amplitudes in the range of 60-70dB, which are the footprints of fiber breaks. Figure 9 (c) presents a different form of amplitude distribution for CNT fibers compared to the neat RTM6-2 sample and T700S carbon fiber composite. This aspect is still unexplained.

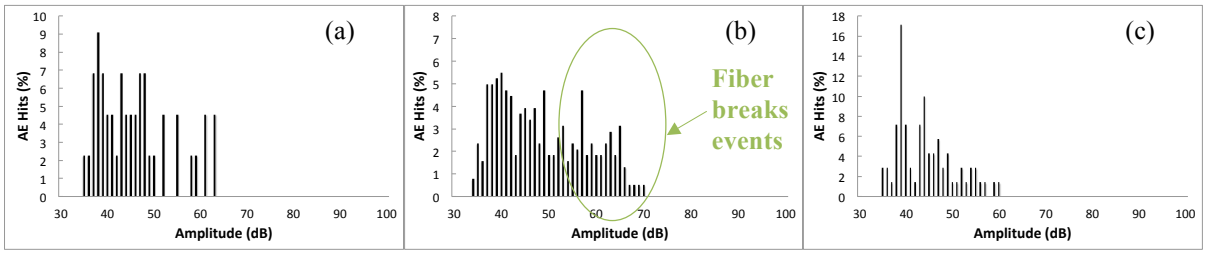

Figure 10. Acoustic emission amplitude versus total acoustic emission hits in percent for neat RTM6-2 sample (a), T700S single fiber/RTM6-2 composites (b) and CNT single fiber/RTM6-2 composites (c)

4 Conclusion

Interfaces between RTM6-2 matrix and T700S carbon fibers or direct-spinning-made CNT fibers have been investigated.

As expected, treated and sized T700 fibers exhibit a strong interface with the epoxy matrix as observed by optical microscopy. CNT fibers seem also to interact very strongly with epoxy. Indeed, CNT bundles are well impregnated by RTM6-2 upon curing leading to the formation of a microcomposite at the fiber-matrix interface.

Acoustic emission analyses reveal quite different behaviours for epoxy/T700S fibers and epoxy/CNT fibers systems. These observations may be attributed to different tensile ability and failure modes for carbon and CNT fibers. To draw additional conclusions and then to retrieve quantitative measurements of interfacial shear stress, new experiments have to be performed on a less emissive and less brittle polymer matrix.

Acknowledgements

This research is carried out within the European FP7 project called Innovative Material Synergies & Composite Processing Strategies (IMS&CPS). Thanks are also due to University of Cambridge (Dr. Fiona Smail and Prof. Alan H. Windle) and Toray CFE S.A. for supplying the fiber materials.

References

[1] Coleman J.N., Khan U., Blau W.J., Gun'ko Y.K. Small but strong: A review of the mechanical properties of carbon nanotube-polymer composites. *Carbon*, **44**, pp. 1624-1652 (2006).

[2] Spitalsky Z., Tasis D., Papagelis K., Galiotis C. Carbon nanotube-polymer composites: Chemistry, processing, mechanical and electrical properties. *Progress in Polymer Science*, **35**, pp. 357-401 (2010).

[3] Sun L., Warren G.L., Sue H.J. Partially cured epoxy/SWCNT thin films for the reinforcement of vacuum-assisted resin-transfer-molded composites. *Carbon*, **48**, pp. 2361-2380 (2010).

[4] Cheng Q.F., Wang J.P., Wen J.J., Liu C.H., Jiang K.L., Li Q.Q., Fan S.S. Carbon nanotube/epoxy composites fabricated by resin transfer molding. *Carbon*, **48**, pp. 260-266 (2010).

[5] Chou T.W., Gao L., Thostenson E.T., Zhang Z., Byun J.H. An assessment of the science and technology of carbon nanotube-based fibers and composites. *Composites Science and Technology*, **70**, pp. 1-19 (2010).

[6] Park J., Lee K.H. Carbon nanotube yarns. *Korean Journal of Chemical Engineering*, **29**, pp. 277-287 (2012).

[7] Koziol K., Vilatela J., Moisala A., Motta M., Cunniff P., Sennett M., Windle A. High-performance carbon nanotube fiber. *Science*, **318**, pp. 1892-1895 (2007).
[8] Zhang X., Li Q., Tu Y., Li Y., Coulter J.Y., Zheng L., Zhao Y., Jia Q., Peterson D.E., Zhu Y. Strong carbon-nanotube fibers spun from long carbon-nanotube arrays. *Small*, **3**, pp. 244-248 (2007).
[9] Behabtu N., Green M.J., Pasquali M. Carbon nanotube-based neat fibers. *Nano Today*, **3**, pp. 24-34 (2008).
[10] Zhong X.H., Li Y.L., Liu Y.K., Qiao X.H., Feng Y., Liang J., Jin J., Zhu L., Hou F., Li J.Y. Continuous multilayered carbon nanotube yarns. *Advanced Materials*, **22**, pp. 692-696 (2010).
[11] Jia J., Zhao J., Xu G., Di J., Yong Z., Tao Y., Fang C., Zhang Z., Zhang X., Zheng L., Li Q. A comparison of the mechanical properties of fibers spun from different carbon nanotubes. *Carbon*, **49**, pp. 1333-1339 (2011).
[12] Filleter T., Bernal R., Li S., Espinosa H.D. Ultrahigh Strength and Stiffness in Cross-Linked Hierarchical Carbon Nanotube Bundles. *Advanced Materials*, **23**, pp. 2855-2860 (2011).
[13] Zhao H., Zhang Y., Bradford P.D., Zhou Q., Jia Q., Yuan F.G., Zhu Y. Carbon nanotube yarn strain sensors. *Nanotechnology*, **21**, pp. 1-5 (2010).
[14] Li Q., Li Y., Zhang X., Chikkannanavar S.B., Zhao Y., Dangelewicz A.M., Zheng L., Doorn S.K., Jia Q., Peterson D.E., Arendt P.N., Zhu Y. Structure-dependent electrical properties of carbon nanotube fibers. *Advanced Materials*, **19**, pp. 3358-3363 (2007).
[15] Herrera-Franco P.J., Drzal L.T. Comparison of methods for the measurement of fibre/matrix adhesion in composites. *Composites*, **23**, pp. 2-27 (1992).
[16] Deng F., Lu W., Zhao H., Zhu Y., Kim B.S., Chou T.W. The properties of dry-spun carbon nanotube fibers and their interfacial shear strength in an epoxy composite. *Carbon*, **49**, pp. 1752-1757 (2011).
[17] Zu M., Li Q., Zhu Y., Dey M., Wang G., Lu W., Deitzel J.M., Gillespie Jr. J.W., Byun J.H., Chou T.W. The effective interfacial shear strength of carbon nanotube fibers in an epoxy matrix characterized by a microdroplet test. *Carbon*, **50**, pp. 1271-1279 (2012).
[18] Li Y.L., Kinloch I.A., Windle A.H. Direct spinning of carbon nanotube fibers from chemical vapor deposition synthesis. *Science*, **304**, pp. 276-278 (2004).
[19] Nielsen A. Acoustic emission source based on pencil lead breaking. *The Danish Welding Institute Publication*, **80**, pp. 15 (1980).
[20] Deng S., Ye L., Mai Y.W., Liu H.Y. Evaluation of fibre tensile strength and fibre/matrix adhesion using single fibre fragmentation tests. *Composites Part A*, **29A**, pp. 423-434 (1998).
[21] Kim B.W., Nairn J.A. Observations of fiber fracture and interfacial debonding phenomena using the fragmentation test in single fiber composites. *Journal of Composite Materials*, **36**, pp. 1825-1858 (2002).
[22] Motta M., Moisala A., Kinloch I.A., Windle A.H. High performance fibres from 'dog bone' carbon nanotubes. *Advanced Materials*, **19**, pp. 3721-3726 (2007).
[23] Mora R.J., Vilatela J.J., Windle A.H. Properties of composites of carbon nanotube fibres. *Composites Science and Technology*, **69**, pp. 1558-1563 (2009).
[24] Vilatela J.J., Khare R., Windle A.H. The hierarchical structure and properties of multifunctional carbon nanotube fibre composites. *Carbon*, **50**, pp. 1227-1234 (2012).
[25] Godin N., Huguet S., Gaertner R., Salmon L. Clustering of acoustic emission signals collected during tensile tests on unidirectional glass/polyester composite using supervised and unsupervised classifiers. *NDT&E International*, **37**, pp. 253–264 (2004).